

See discussions, stats, and author profiles for this publication at: <https://www.researchgate.net/publication/231647327>

# Study of the Attachment of Linker Molecules and Their Effects on the Charge Carrier Transfer at Lead Sulfide Nanoparticle Sensitized ZnO Substrates

ARTICLE *in* THE JOURNAL OF PHYSICAL CHEMISTRY C · JUNE 2011

Impact Factor: 4.77 · DOI: 10.1021/jp200935x

---

CITATIONS

18

READS

47

## 4 AUTHORS, INCLUDING:



Stephen G Hickey

University of Bradford

75 PUBLICATIONS 2,248 CITATIONS

[SEE PROFILE](#)



Alexander Eychmüller

Technische Universität Dresden

356 PUBLICATIONS 10,776 CITATIONS

[SEE PROFILE](#)

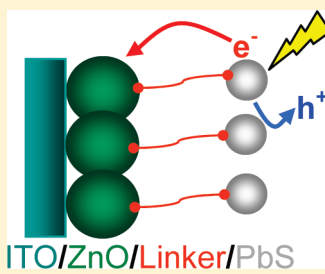
# Study of the Attachment of Linker Molecules and Their Effects on the Charge Carrier Transfer at Lead Sulfide Nanoparticle Sensitized ZnO Substrates

Susanne Krüger, Stephen G. Hickey,\* Stefanie Tscharntke, and Alexander Eychmüller

Physical Chemistry/Electrochemistry, TU Dresden, Bergstrasse 66b, D-01062 Dresden, Germany

 Supporting Information

**ABSTRACT:** In order to attach nanoparticles to substrates using solution based assembly methodologies, one invariably relies on linking molecules whose importance is not solely as the binding component between the semiconductor substrate and the nanocrystal but also as an important in-series component in any charge carrier transfer (CCT) processes occurring in the circuit. The role of these linker components and their exact influence on CCT is presently ambiguous. In the present work a substrate consisting of ITO/ZnO/linking molecule (linker) onto which PbS nanocrystals (NCs) have been covalently bound is characterized. In this study a great deal of emphasis has been placed on the role of the linker, and it is shown that the linker is a major key to the understanding of the CCT processes and has an important influence by not only transferring or blocking the electron and hole intermediates in such systems but also making its own inherent and often substantial contribution to the optoelectronic response. To gain a greater understanding concerning the complex roles played by the linker, a number of different molecules with different functional groups and different alkyl chain lengths were used to connect the NCs to the ZnO layer, with the attachment of the linkers and NCs to the ZnO substrate being verified by spectroscopic methods and the optical and optoelectronic response being studied. In addition the results presented allow the possibility to propose a model for how the linker and NCs interact spatially and electrochemically with the ZnO layer.



## INTRODUCTION

The prime reason for the importance and widespread use of semiconductors in many applications is their band structure. Upon publication of the utilization of wide band gap materials in a dye sensitized solar cell (DSSC) by O'Regan and Grätzel,<sup>1</sup> research into thin films of semiconducting oxides for use in clean and renewable energy conversion systems re-entered a period of intense research. Although TiO<sub>2</sub> is the most employed oxide substrate for DSSC cells, a number of other oxidic semiconductors of note are reported in the literature, among which are SnO<sub>2</sub>, ZnO, Nb<sub>2</sub>O<sub>5</sub>, and In<sub>2</sub>O<sub>3</sub>.<sup>2–9</sup> The energetically wide band gap of these materials<sup>10</sup> makes it possible to control the transfer of the electron from the excited state of the absorber, the dye in the case of a DSSC, to the substrate and transfer of the hole to a solution species. Consequently the electron and hole become separated if the relative positions of the electronic states of the sensitizer are judiciously positioned with respect to those of the conduction band of the semiconductor and the hole acceptor. The search therefore for the best sensitizer, i.e., one which can efficiently absorb as much of the solar spectral output as possible while at the same time being electronically "well matched" to the substrate material, is an active area of research.

Semiconductor nanocrystals (SCNC) have received a great deal of attention not only because of their absorption and emission properties but also because these properties may be "tuned" across a wide spectral range. A number of SCNC materials presently exist which can controllably and reproducibly be synthesized and, in combination, can be made to address a large spectral range from the

visible to the near infrared (NIR). By removing portions of the growth mixture at different times throughout a nanocrystal synthesis one can obtain an SCNC material of a number of different sizes and therefore material which has been tuned to be active in a number of different regions of the spectrum. One very important consequence of the fact that the materials can have their optical properties tuned is that the material remains in essence chemically identical and therefore has effectively the same composition and chemistry. This has the major advantage that any chemical modification that has been successfully applied to one size can usually be further applied to any other. This is unlike the case for dyes, where the optically active centers are molecular, and therefore, to change the optical properties one must engineer the molecule, which is by its very nature a more challenging prospect and once achieved still only allows one characteristic absorption and emission profile.

The optoelectrical properties of quantum sized particles, especially those of the metal chalcogenides, e.g., MX species (where M = cadmium, zinc, or lead and X = sulfur, selenium, or tellurium) are most common because of the size of their band gap<sup>11–15</sup> and their relative band positions as compared to those of the semiconductor oxide states. Already, the TiO<sub>2</sub>/CdSe<sup>16–19</sup> and TiO<sub>2</sub>/CdTe<sup>20–23</sup> systems have been successful fabricated and many of the anomalies reported upon.<sup>24</sup> Much interest in the

**Received:** July 26, 2010

**Revised:** May 18, 2011

**Published:** May 18, 2011

lead chalcogenides has been generated by reports that they possess the possibility to exhibit multiple exciton generation (MEG) and where it has been demonstrated that absorption of one high energy photon in such materials can result in more than one electron–hole pair.<sup>25–31</sup>

A spectral region so far difficult to address with organic dyes is the infrared, particularly the region which is greater than approximately 950 nm. In this region it has so far proven to be problematic to synthesize dyes which are both electronically suitable and stable, the latter proving to be especially challenging. A number of SCNC materials possess band gaps that are well suited to addressing this region of the spectrum among which are InAs and Cd<sub>3</sub>P<sub>2</sub> and the lead chalcogenides PbS, PbSe, and PbTe. These materials can therefore in principle be utilized to allow the harvesting efficiency of the solar spectrum to be increased if they are employed as absorbers in regions where dyes, up until now, have been unable to adequately address. However one must still design the electronic structure of these materials to match that of the substrate. In vacuum, the conduction band of bulk ZnO and TiO<sub>2</sub> is located at 4.2 eV while that of bulk PbS is 4.74 eV below the vacuum level. Vogel et al.<sup>32</sup> have shown that sensitization of TiO<sub>2</sub> with PbS quantum dots of between 3 and 6 nm in size can be utilized to bring about the separation of the electron–hole pair. Hence by tuning the PbS band gap, i.e., stopping the growth of the NCs when they are in this size regime, the electron transfer to the substrate becomes energetically feasible. Therefore, all of the essential components for the fabrication of quantum dot sensitized solar cell (QDSSC) devices<sup>33</sup> exist, and a number of such devices have been reported.<sup>24</sup>

In this work the optical and optoelectrochemical responses of a number of ZnO-linker-PbS systems is reported. Attempts at optimization of the optical response were primarily focused on changing the linker molecule, specifically by varying the alkyl chain length and the choice of either acid and/or thiol groups employed as the attachment moieties at the linker ends. Analyses of linker influences in QDSSCs have been reported for nanoparticle sensitized TiO<sub>2</sub> electrodes. TiO<sub>2</sub> sensitized with CdSe and CdS nanoparticles has been especially examined for linker dependency and attachment mode using optical, incident photon to current efficiency (IPCE), photo transients, and ultrafast carrier dynamic techniques.<sup>19,34,35</sup> In the present work the electrochemical and optoelectrochemical measurements especially those of cyclic voltammetry, electrochemical impedance spectroscopy (EIS), and photocurrent spectroscopy were employed to gain insights into the different interactions between the components, the relative efficiencies of exciton separation, and material stabilities. Additionally analysis of the substrate was carried out using UV-vis, Fourier-transform infrared (FTIR), and X-ray diffraction (XRD) spectroscopies to give insights into material composition and the nature of the molecular contact characteristics.

## ■ EXPERIMENTAL SECTION

**Materials.** For the PbS synthesis the following materials were used: bis(trimethylsilyl)sulfide (purum, Fluka), butanol (p.A., AppliChem), dimethylformamide anhydrous (99.8%, Aldrich), diphenylether (>98%, Acros), lead acetate (99.999%, Sigma-Aldrich), oleic acid (90%, Aldrich), thioacetamide (>99+ %, Sigma-Aldrich), tetrachlorethylene (anhydrous 99+ %, Sigma-Aldrich), toluene (p.A.), trioctylphosphine (90%, Fluka). For the

PbS synthesis all chemicals were used as received with the exception of TOP which was doubly distilled.

ZnO was synthesized using zinc acetate (Zn(Ac)<sub>2</sub>, 99.99%, Aldrich), lithium hydroxide monohydrate (LiOH·H<sub>2</sub>O, 98%, Aldrich), and dry ethanol (SeccoSolv, Merck). The molecules employed in this study to link the PbS nanoparticles to the ZnO were thioacetic acid (TAA, 96%, Aldrich), thioglycolic acid (TGA, >98%, Fluka), mercaptopropionic acid (MPA, >98%, Fluka), hexandithiol (HDT, >97%, Fluka), oxalic acid (OA, 99%, KMF), and malonic acid (MA, 99%, AppliChem). As conducting substrate indium tin oxide (ITO, Merck, Sheet Resistance ≤ 20 Ω/sq) was used. The preparation of the ZnO-linker-PbS substrates was carried out from solutions in tetrahydrofuran (THF, Acros Organics). All water used was purified using a Milli-Q system and had a resistance of ≥ 18.2 MΩ.

**PbS Nanocrystal Synthesis.** The PbS nanocrystals were synthesized in a three-necked flask under an inert atmosphere of N<sub>2</sub>. A mixture of lead acetate (2 mmol), 1.5 mL of oleic acid (4.4 mmol), 2 mL of diphenylether (12.6 mmol), and 8 mL of trioctylphosphine (17.9 mmol) was heated under vacuum for 1 h at 80 °C to form lead oleate. The resulting clear and colorless solution was then heated to the injection temperature (140 °C), and a mixture of 0.1 mL of thioacetamide (0.67 mmol), 0.1 mL of bis(trimethylsilyl)sulfide (0.53 mmol), and 6 mL of trioctylphosphine (13.4 mmol) was injected. The color changed instantly to black, and after a growth time of 10 min, the solution was cooled down to room temperature. For the cleaning-up procedure the particles were precipitated twice using butanol and redissolved in toluene. For spectroscopic investigations solutions of the nanocrystals in tetrachloroethylene were used.

**ZnO Synthesis and Preparation of the Substrate.** The ZnO synthesis employed was a modification of that described by Spanhel and Anderson<sup>36</sup> and optimized by Meulenkamp et al.<sup>37</sup> The ZnO synthesis protocol was carried out under inert atmosphere conditions (Ar) using water free chemicals, and hence, the necessity for the boiling step was circumvented. In a typical synthesis Zn(Ac)<sub>2</sub> (1.464 g, 5 mmol) was dissolved in dried ethanol (75 mL/59.2 g) while stringently maintaining the oxygen and water free conditions. A LiOH·H<sub>2</sub>O/ethanol solution (0.455 g, 7 mmol/75 mL) was prepared, and the injection of this solution was performed at a temperature of ≤ 2 °C. Subsequently, the resulting clear solution was refluxed for 10 min at 65 °C. After heating the solution Milli-Q water was quickly added for as long as a precipitation was observed to occur. This treatment was followed by washing the ZnO gel three times with an ethanol/water mixture (95:5). The resultant ZnO was then spin coated onto an ITO coated glass substrate which had previously been boiled in a 5% Extran-solution for approximately 15 min. After sintering, the ZnO-substrate was placed into a solution of the linker in THF (0.2M) for approximately 4 h. Subsequently, the substrate was washed with THF and then added to a solution of the PbS nanoparticles in THF (0.0002 mM) for 12 h. The substrate may thus be visualized to be composed of a layer by layer structure whereby the PbS is bound to the ZnO layer through different structured linkers (Figure 1).

**Characterization of the Substrate.** UV-vis absorption spectra of the substrate were collected using a Cary 5000 spectrophotometer (Varian). FTIR spectra were recorded on a Nicolet 5700 FTIR spectrometer (Thermo) after it had been degassed for 30 min with N<sub>2</sub>. The number of scans recorded was 200. The X-ray diffraction (XRD) measurements were carried

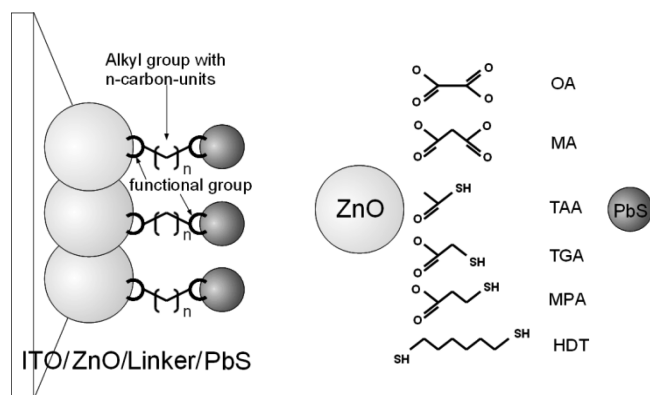


**Figure 1.** (Right) Schematic of the ITO/ZnO/linker/PbS substrate used in these studies. The substrate consists of PbS nanoparticles which are bound by a linker molecule to ZnO which has been spin-coated onto ITO glass. The linker molecules vary in their alkyl-chain and functional groups. (Left) Structures representing the linker molecules used in the study: oxalic acid (OA), malonic acid (MA), thioacetic acid (TAA), thioglycolic acid (TGA), mercaptopropionic acid (MPA), and hexanedithiol (HDT).

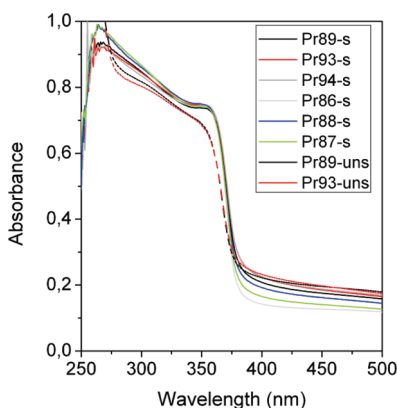


**Figure 2.** UV-vis spectra of sintered ZnO-layers (PrX-s where X is an internal sample reference number) on ITO. The sintering results in a slight red shift of the peak and an increase in the absorption when compared with the unsintered ZnO-layers (PrX-uns).

out on a D5000 diffractometer (Siemens, Cu K $\alpha$  radiation). For all measurements of the ZnO/linker/PbS layered structures ITO was used as the substrate support. Only in the case of the reference XRD measurement of the PbS nanoparticles was this altered and a Si wafer used as the substrate.

SEM images were taken on a Zeiss Gemini 982 spectrometer with a thermal field emission cathode. The optoelectrochemical measurements were undertaken using a Zahner IM6 equipped with a CIMPS (XPOT) system. The LED used for illumination had a peak intensity at 470 nm and was powered using a BUVZ01 integrated LED light source system. The illumination intensity range, across which the intensity response was linear, was determined, and in this study, an illumination intensity of 10 W/m<sup>2</sup>, which was within this linear region, was used. A Pt-sheet was utilized as a counter electrode, and a 0.1 M sodium sulfite solution, a well established hole scavenger,<sup>38–42</sup> was employed as the background electrolyte with an Ag/AgCl/3 M NaCl electrode being used as the reference. All electrochemical potentials reported within are relative to this reference electrode.

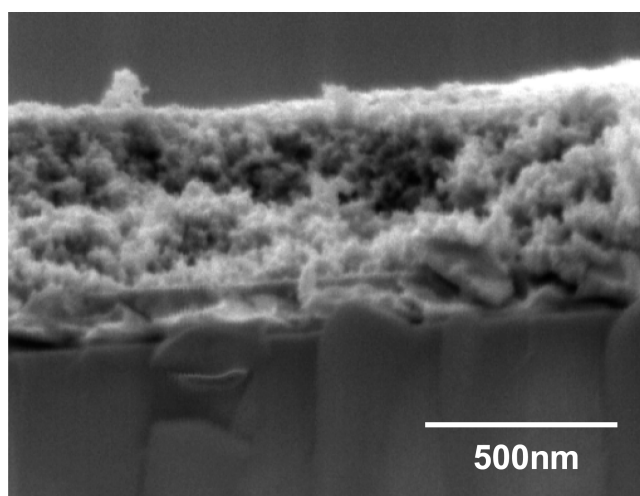


**Figure 3.** SEM image of a 400 nm thick homogeneous nanoporous ZnO layer on ITO.

## RESULTS AND DISCUSSION

The synthesis of the ZnO resulted in a colorless gel with an absorption onset at 380 nm and which generated a broad emission band at 540 nm as a result of trap and defect states.<sup>36,43</sup> The yellow emission results from incorporation of lithium, which acts as an acceptor, into the ZnO, the lithium initially being present during the synthesis.<sup>44</sup>

The reproducibility of the ZnO thickness of each sample was verified using UV-vis spectra (Figure 2). A slight increase and red shift of the ZnO absorption was observed to occur after sintering which is in agreement with previous studies.<sup>45</sup>

From SEM images the ZnO films were confirmed to be homogeneous and have a thickness of between 300 and 400 nm. From the images (Figure 3) it may also be observed that the layers have a nanoporous structure.

The porous topology is formed from a loosely packed structure of small ZnO nanocrystals. From further SEM images (not presented), an average ZnO crystallite diameter of 10 nm has been measured. Earlier studies on ZnO layers have shown equivalent particle sizes and ZnO layer properties<sup>45</sup> as well as a thickness dependence of the photocurrent transient profiles for such systems.<sup>46</sup>

As knowledge concerning the attachment and orientation of the linker at the ZnO interface is of utmost importance for the attachment of the nanoparticles and impacts greatly on the charge carrier transfer rates, an FTIR study of the linker molecules on ZnO was undertaken. The ITO/ZnO substrates were immersed in a solution of the linker, and after immersion, the FTIR spectra of the ITO/ZnO/linker systems were taken and found to possess significant signals related to the alkyl and acid groups (see Figure 4). The FTIR peak associated with thiol groups is expected to be in the region from 2600 to 2550 cm<sup>-1</sup>. Most likely as a result of low concentration at the ZnO surface, which is expected to be at best monolayer coverage, and the generally low peak intensity associated with the thiol-group stretching signature, no signal for these functional groups was ascertainable in the FTIR spectra (see Table 1 in Supporting Information for all expected signals and their associated vibrations).

In the region around 3200 cm<sup>-1</sup> broad bands were obtained from linker molecules containing acid groups. If the assumption

that the carboxylic acid functional group is attached to the ZnO-surface and the second functional group is pendant into the solution is correct, then it is possible that the nonbonded carboxylic acid groups of the dicarboxylic acids can form mutual H-bonds.<sup>47</sup> The H-bonds of the OA and MA molecules and the strong pH-dependence of their spectra are well documented.<sup>48</sup> It is also documented in the literature which parts of the OA and MA acid group are bound to the surface of TiO<sub>2</sub>,<sup>49</sup> CrO<sub>50</sub> and kaloinite,<sup>51</sup> and no deviances from the reported behavior are to be intuitively expected in this study. The connection of the dicarboxylic acids to the surface of the ZnO as ions is further confirmed by the presence of bands at 1639, 1479, and 1361 cm<sup>-1</sup> in the case of OA<sup>52</sup> and 1628, 1448, 1421, and 1381 cm<sup>-1</sup> for MA (Figure 5B). Hanrahan et al.<sup>53</sup> have ascribed the peak shift that arises for MA to be due to the dissociation of the carboxylic acid groups. Hence the peaks present at approximately 1600 cm<sup>-1</sup> may be attributed to that of COO groups whereas the signature that appears at around 1700 cm<sup>-1</sup> is the signature associated with the COOH groups. The presence of a signal at 1709 cm<sup>-1</sup> in the case of OA (Figure 5A) also gives an indication that some carboxyl groups (e.g., the C=O bond) are still present.

The TAA molecules (Figure 5C) can link to the surface via the C=O functionality. The strong bands at 3200, 1654, and 1631 cm<sup>-1</sup> are evidence of C—O— bonds (dissociated OH-groups) through which the linking to the surface occurs.

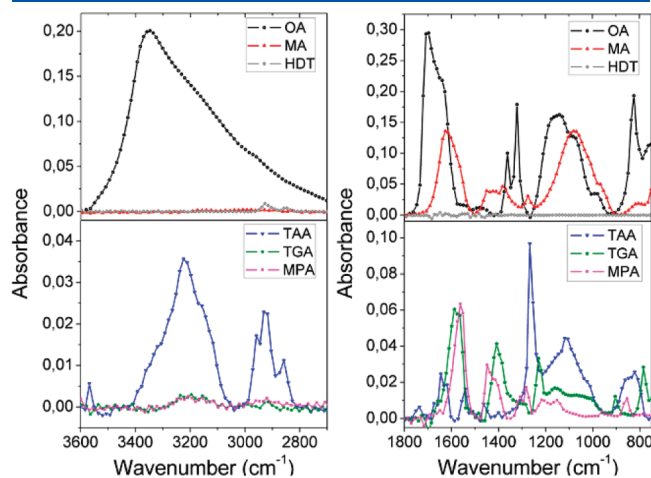


**Figure 4.** FTIR spectra, in the ranges 3600–2700 cm<sup>-1</sup> (right) and 1800–750 cm<sup>-1</sup> (left), of the linkers on the ZnO-layer.

Because the oxygen is bound to the oxide surface the vibration signal shows a slight shift compared to that of the C=O stretches of the TAA, which have been reported in the literature to occur at 3360 and 1696 cm<sup>-1</sup>.<sup>54,55</sup> Also present are signals with a high intensity associated with the CH stretching vibrations at 2900 and 2800 cm<sup>-1</sup> due to the presence of methyl groups. By comparison to the CH<sub>3</sub> group present in the TAA, the CH stretching vibrations of the HDT molecule can only be due to CH<sub>2</sub> groups as only these are present within the alkyl chain. TGA (Figure 5D) shows a dominant carboxylate linking to the surface which is confirmed through the presence of a weak signal at 3200 cm<sup>-1</sup>. The signal at 1587 cm<sup>-1</sup> provides evidence of a dissociated acid group. The MPA (Figure 5E) linker which contains an even higher number of CH<sub>2</sub> groups than TGA is also attached to the ZnO only by the carboxylate group. This linker shows significant signals at 1562 cm<sup>-1</sup> for COO groups and also has a weak signal at 3200 cm<sup>-1</sup>. As expected it was not possible to observe the C—S signal at approximately 650 cm<sup>-1</sup> for the substrate covered with the HDT-linker (Figure 5F) due to its very weak intensity (see Table 1 of FTIR peak assignment in Supporting Information). As a result of the FTIR study it may therefore be proposed that the connection of the linkers to the ZnO surface is that as represented in Figure 5. In previous reports, the electron transfer of a number of linker molecules with various alkyl chain lengths was studied using STM and optical, kinetic, and electrochemical measurements. It was demonstrated that the molecular interactions within the film, the type of assembly, the molecular structures, and the bond between substrate and linker have the most important influence on the electron transfer in the system.<sup>56–61</sup> Thus, the identification of the particular mode of attachment that the linkers employed in this study have and their influences, specifically on charge carrier transfer, is of some importance.

Attempts to measure the PbS nanoparticles after their attachment to the ZnO surface via XRD yielded diffractograms dominated by the intense diffraction peaks of the ITO, and therefore, a clear XRD signal associated solely with the presence of the PbS could not be unambiguously recorded. However, the UV-vis-NIR spectra of a number of samples were found to possess a low intensity PbS signal when a sufficient amount of the material was present.

In Figure 6 the UV-vis-NIR spectrum gained upon the addition of each layer is presented. For the ITO-ZnO-linker-PbS substrate a weak absorption shoulder in the NIR can be observed

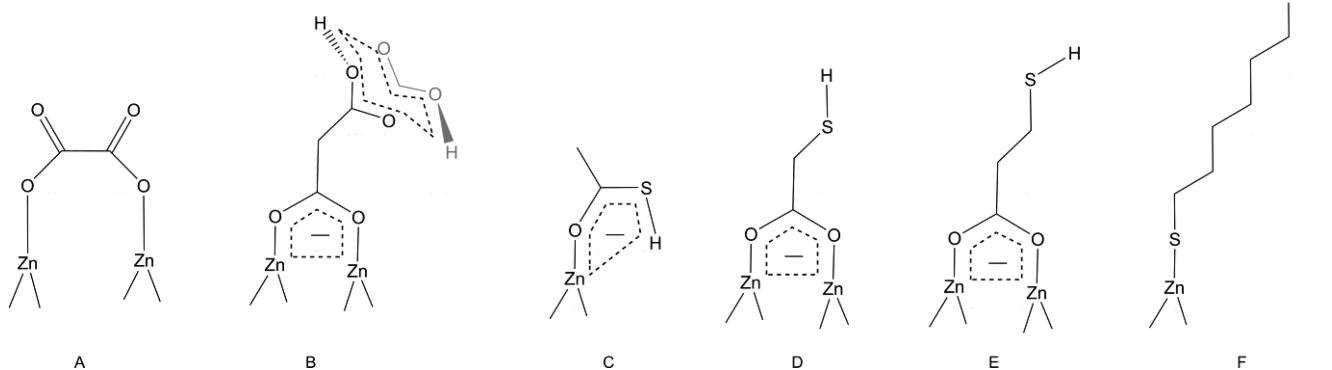


**Figure 5.** Schematic of the proposed linker bonding modes to the ZnO substrate: A, OA; B, MA, C, TAA; D, TGA; E, MPA; and F, HDT.

that matches the position of the solution phase absorption maxima of the PbS nanoparticles. Similarly, it was by the visible changes in the ITO/ZnO/linker substrates that occurred after immersion into the nanoparticle solution that indications concerning the degree of PbS present after the coating procedure could be primarily derived. For the substrates with only linker molecules attached to the sintered ZnO-layer, there are no changes discernible by eye (top portion of substrates in Figure 7). The sintered ZnO-layers have been measured to have an absorbance of approximately 20% when compared with a bare ITO substrate (see Figure 6b). After immersion of the substrates in the THF solution containing PbS NCs, the substrates were observed to show a clear color change from being almost transparent but possessing a slight tint to a distinct brown coloration (bottom portion of substrates in Figure 7). The degree of the coloration provides a visual aid as to the amount of PbS absorbed on the surface. However, it must be mentioned that the degree of coloration at the surface of the ZnO is not necessarily a trustworthy indicator of the level of the optoelectrochemical response that one measures under conditions of illumination, as will be more fully discussed below. The solution containing the OA-linker was found to have a very high interaction with the ZnO layer which was observed to be displaced partially from the ITO substrate during the immersion step and resulted in "crumblike" agglomerates on the ITO (Figure 7, substrate A).

The use of dynamic electrochemical methods such as cyclic voltammetry provides a means to investigate surface species at

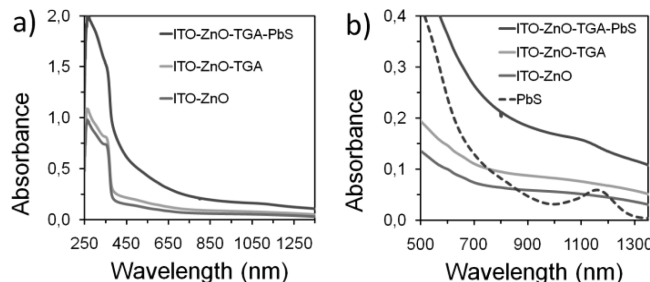


**Figure 6.** (a) UV-vis spectra of ITO substrates coated with ZnO, ZnO-TGA, and ZnO-TGA-PbS using a bare ITO substrate as reference and (b) as for part a but in the wavelength range not dominated by the ZnO absorbance and with the inclusion of the absorbance of the PbS nanoparticle solution in tetrachlorethylene for comparison.

the electrode/electrolyte interface and hence was employed here to, among other things; confirm the presence of the PbS NCs.

The electrochemical response for all of the ITO-ZnO-linker systems employed in this study was observed to result in a current of less than  $5 \mu\text{A}/\text{cm}^2$  across the potential range from  $-1.2$  to  $0.4$  V using  $0.1$  M sodium sulfite as background electrolyte. In electrochemical studies in the dark and where scans more negative than  $-1.2$  V were required the background electrolyte employed was sodium perchlorate due to its greater inertness at such negatively applied potentials (more details on this issue are provided in the Supporting Information). In  $\text{Na}_2\text{SO}_3$  a linear decrease in the reduction current begins at  $-0.3$  V and is similar for both the ITO and ITO-ZnO substrate. Rifai et al.<sup>62</sup> have previously published cyclic voltammetry studies on HDT where the presence of well-defined signals was reported. However, the oxidation of the linker samples observed in the present work is not as pronounced. The cyclic voltammetry also provided a clear indication that the coverage of the ZnO by the linker molecules was total, as for all ITO-ZnO-linker substrates the expected electrochemical signature for ZnO at  $-0.7$  V and  $-1.15$  V was completely suppressed (Figure 9b). Upon deposition of the PbS NCs, however, the CV profiles are observed to be dramatically altered. This influence can be seen in Figure 8 where three voltammetric sweeps of ITO-ZnO-linker-PbS, for three different linkers, are presented. As can be clearly observed the signal decreases with each successive voltammetric sweep in the oxidation potential direction as well as the reduction direction.

In Figure 9a the first sweep of the characteristic reaction of the complete ZnO-linker-PbS systems is illustrated for all linkers. The detailed electrochemical reactions of bulk PbS have previously been reported in the literature. Such studies focus primarily on bulk galena where a strong pH dependence of the signal position has been shown to exist.<sup>63–67</sup> Previous studies on quantum sized PbS<sup>68</sup> have ascertained the existence of the influence of the quantum size effect on the redox potential. Hence the presence of a wider band gap resulting from the decrease in the size of the PbS nanoparticles results in a shift to more negative potentials of the reduction peaks as a result of the differences in the electronic position of the conduction band. A complementary shift was observed for the anodic scan. The oxidation peak "A" in Figure 9a is obtained even if previously the reduction potential had not been passed through. The reaction therefore cannot be mediated via a previously reduced species and therefore must be due to the direct oxidation of the PbS in

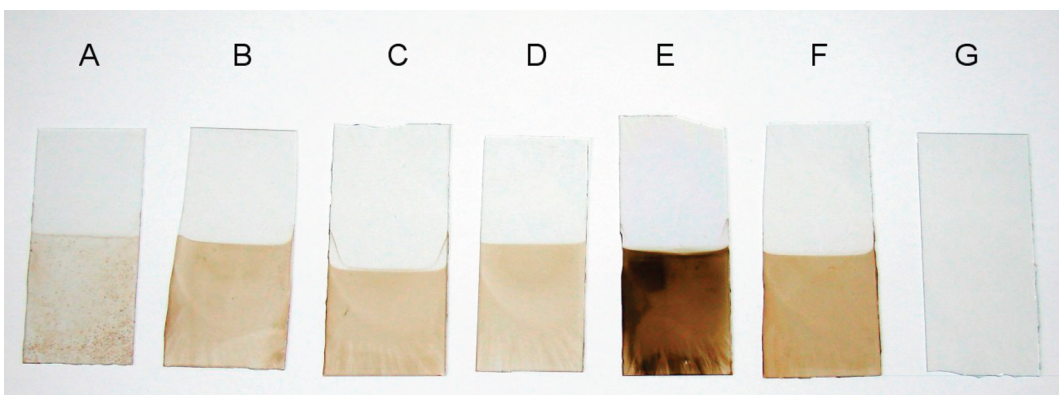


**Figure 7.** ZnO only (G) and ZnO-linker molecule-PbS (A–F, top portions) look similar and have a slightly reflective but predominantly transparent surface. In contact with the PbS the substrate color will take on a brown coloration from the PbS (A–F, bottom portions). The linker molecules are A, OA; B, MA; C, MPA; D, HDT; E, TAA; and F, TGA.

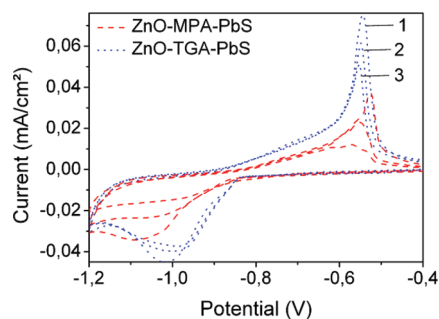


**Figure 8.** Cyclic voltammogram of the ZnO-MPA-PbS, ZnO-TGA-PbS, in the range from  $-1.2$  until  $-0.4$  V for three voltammetric sweeps of each linker system.

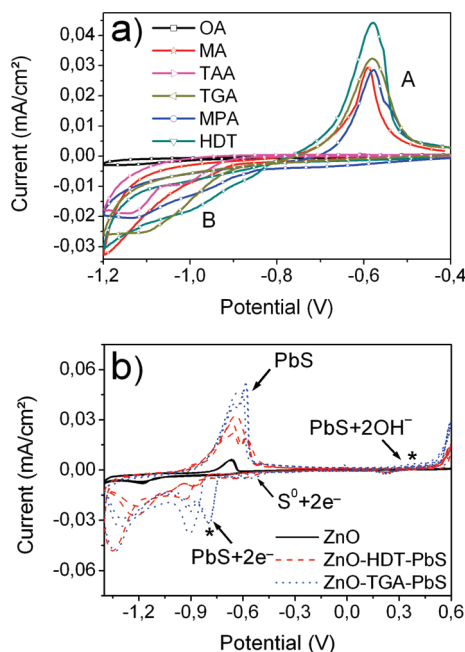
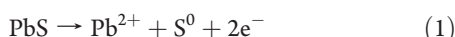


**Figure 9.** (a) Cyclic voltammogram of the ZnO-linker-PbS system in  $\text{Na}_2\text{SO}_3$  under conditions of nonillumination in the range from  $-1.2$  until  $-0.4$  V. (b) Cyclic voltammogram of the ZnO, ZnO-HDT-PbS, and ZnO-TGA-PbS in the range between  $-1.4$  and  $0.6$  V in  $\text{NaClO}_4$  solution ( $\text{pH} = 12$ ) for three voltammetric sweeps. The asterisks mark the position of the reduction peak at approximately  $-0.8$  V and the beginning of the oxidation peak at approximately  $+0.4$  V.

the electrolyte. Experiments undertaken separately on an ITO-ZnO-linker substrate demonstrate that this oxidation peak is only observed when the PbS layer is present. The oxidation reaction can be ascribed to the following reaction:<sup>63,65</sup>



No such signal is detected for PbS systems where either the TAA or OA linker is present on the ZnO layer. As previously mentioned, during the OA coating procedure it was observed that the ZnO is at least partially removed from the ITO surface. There is therefore a smaller amount of ZnO present at the ITO surface which consequently results in a smaller amount of PbS being present. Also, if the linker molecules are attached as proposed in Figure 6, there is no acidic proton present to undergo dissociation and provide an attachment site for the PbS NCs. Unusually, as can be seen from

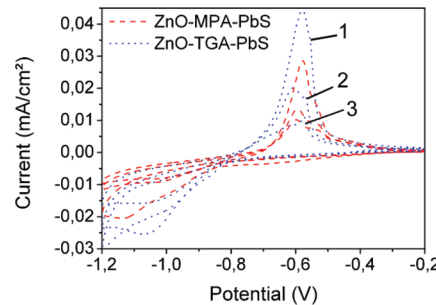
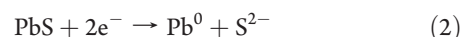


**Figure 10.** Cyclic voltammogram of ZnO-MPA-PbS and ZnO-TGA-PbS in the range  $-1.2$  to  $-0.2$  V in  $\text{Na}_2\text{SO}_3$  for two voltammetric sweeps under illumination with blue light.

Figure 7, the “blackest” substrate is that of the TAA derivatized ZnO, and as such, one would therefore have expected that the largest PbS related signature would be recorded for this substrate. In fact for a number of such substrates this was consistently found not to be the case, and presently, further studies to determine the exact nature of this surface species are ongoing.

The potential shift of the redox reaction when compared to that of galena from the literature may be adequately explained by the quantum size effect<sup>68</sup> as well as a possible contribution associated with the influence of the linker contact. A second low intensity oxidation peak between  $0.05$  and  $0.15$  V (this exact value being dependent on the linker present) can be determined only for the first cycle and is much more distinct for the presence of the TGA, HDT, and MPA linker molecules. The product can be attributed to the presence of an impurity caused by the oxidation by air of the PbS species or by the partial stripping of the linker molecules. The large scale conversion of  $\text{Pb}^+$  to  $\text{Pb}(\text{OH})_2$  can be ruled out due to the absence of a white precipitate in the vicinity of the electrode. This is further substantiated by the fact that during the measurement of the same samples in a solution of  $0.1$  M  $\text{NaClO}_4$  at  $\text{pH} 12$  the presence of small amounts of white  $\text{Pb}(\text{OH})_2$  was observed and was accompanied by the presence of a third oxidation peak in the cyclic voltammogram at the expected potential (Figure 9b).<sup>64,69,70</sup>

The reduction peak “B” in Figure 9a at around  $-1.1$  V is likewise decreased with each voltammetric sweep, and it was also noted that there is a linker dependence on the potential position of this peak. This reduction can be assigned to that of metallic lead and is analogous to that found in the studies of Nicol et al.<sup>67</sup> The corresponding weak signal at around  $-0.65$  V is associated with the reduction of sulfide ion.



The signals for this reaction can also be found in measurements taken of the same substrate measured in  $0.1$  M  $\text{NaClO}_4$  at  $\text{pH} 12$  at between  $-0.8$  and  $-0.6$  V and hence are not related to the presence of the sulfite.

The above CV measurements, which had been recorded in the dark, were repeated under conditions of illumination using a blue LED ( $\lambda_{\text{peak}} = 470$  nm). In this case differences in both the position and degree of oxidation and reduction are observed (Figure 10).

The energy difference between the reduction “B” and oxidation “A” peaks in sodium sulfite (Figure 9a) did not correspond to the magnitude of the PbS NC optical band gap, which is approximately  $1.1$  eV as determined from absorbance spectroscopy, an

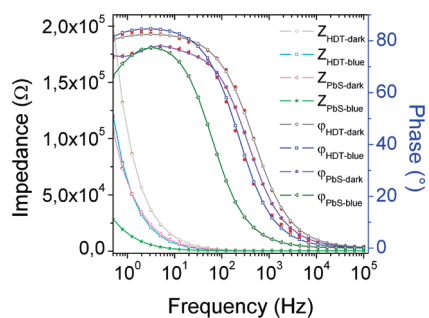


**Figure 11.** Bode diagram of the ITO-ZnO-HDT (red circle, red triangle) and ITO-ZnO-HDT-PbS (red square, red star) substrates in the dark under 470 nm illumination. The fits (line-symbol-line) are in very good agreement with the measured data.

observation that has also been reported elsewhere for CdS<sup>71</sup> and CdTe.<sup>72</sup> However, for CVs recorded using NaClO<sub>4</sub> as background electrolyte an inert electrochemical window between the most positively positioned oxidation peak and the first observed reduction peak, corresponding to a difference slightly larger than 1.1 eV, was observed. The energy positions and width of this potential window were therefore examined to determine if they might be associated with the expected conduction and valence bands of the PbS NCs. The flat potential window is located between -0.8 and 0.5 V. According to Xu et al.,<sup>10</sup> bulk PbS has its CB at -4.74 V and VB at -5.11 V versus the vacuum level. The band positions of PbS NCs with a band gap of 1.1 eV and, as the effective masses of the electron and hole in PbS are equal, a symmetrical change in the band energies are expected whose positions can be calculated using the Brus formula<sup>73</sup> (CB at -4.39 V; VB at -5.49 V). Using 1 M K<sub>3</sub>[Fe(CN)<sub>6</sub>]/K<sub>4</sub>[Fe(CN)<sub>6</sub>] mixture 1:1 the potential of the Ag/AgCl/NaCl (3 M) electrode used was determined to be 0.208 V versus NHE, which corresponds to -4.808 V with respect to the vacuum (a value of -4.6 V<sup>74</sup> was used as the energetic level of the NHE with respect to the vacuum). Therefore, the CB and VB of the PbS NCs were calculated to be -0.68 V and 0.42 V, respectively, versus Ag/AgCl/NaCl (3 M), values which are indeed in good agreement with the measured CV peaks. The difference observed (approximately 0.2 V) may be accounted for as the electrochemical band gap is larger than that of the optical band gap due to the extra energy required to transfer charge across the interface(s).

A more detailed overview of the charge carrier processes in the system as a whole can be obtained using EIS and subsequent analysis by fitting the data to equivalent circuit models. The Bode diagram of the ITO-ZnO-HDT-PbS system presented in Figure 11 is typical. Under conditions of illumination a strong influence was determined which is seen as a shift in the phase (blue) to lower frequencies. Accordingly, the impedance Z is reduced.

From Figure 11 it can be deduced that under conditions of illumination a decrease in the total resistance R and an increase in the sum of the capacitance C was observed. The value of the shift and the influences of R, C, and consequently Z are dependent on the photoactivity of the samples as will be discussed. A fuller interpretation of the data may only be derived through fitting of the data to an equivalent circuit which, as the term suggests, is formulated on the basis of treating the interface as if it were composed of ideal electrical components in combinations of series and/or parallel circuitry. The equivalent circuit used for fitting and the subsequent data derived are presented and discussed in the Supporting Information.

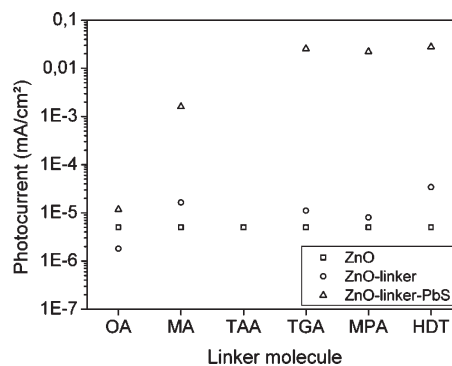


**Figure 12.** Role of the ZnO, linker, and PbS in comparison to the complete ZnO-linker-PbS system.

The degree of photoactivity of each system was obtained by measuring its dc photocurrent response. An overview of the influence that the addition of each stage of the ITO-ZnO-linker-PbS system has on the photocurrent response is presented in Figure 12. The magnitude of the photocurrent for the ZnO/ITO substrates was found to be constant and reproducible having a value of  $8 \times 10^{-9} \text{ A/cm}^2$ . The highest photocurrents were recorded from the MPA, HDT, and TGA linker-PbS systems, and it is of interest that in these systems the linker itself also has a contribution to the sum of the photocurrent. The increase in the photocurrent response after the linker attachment can be explained by the ability of the linker to increase the trap depth of the ZnO through interaction with its dipole moment. The higher the dipole moment of the ligand the higher the possibility to inject an electron into the ZnO surface states which results in the surface states converging toward the CB. The trap states become "lost" when charge injection occurs from ligands containing negatively polarized functional groups.<sup>75,76</sup>

It was also observed that the photocurrents in all of the systems with PbS reached the same upper value (a limiting value of the photocurrent under the conditions employed here). This fact is not intuitively expected given the possible differences in preparation: different linker molecule, differences in surface particle concentration, etc. In previous studies we have found that the electron injection from solution by SO<sub>3</sub><sup>2-</sup> was a slow process and therefore is likely to be among the contributive factors.<sup>39</sup>

The MA system also generates a comparable photocurrent which is in the  $1 \mu\text{A}/\text{cm}^2$  range. The photocurrent response of the OA system may be indicative of a number of the problems encountered in the coating procedure of this linker, a number of which have been previously mentioned. Although no significant photocurrent can be observed for the ZnO alone, ZnO-OA shows even less than this "background" photocurrent due to the dissolution of the ZnO during immersion in the linker solution. The TAA system is only partially presented in Figure 12 as the photocurrent obtained for the ITO-ZnO-TAA-PbS was negative. The photocurrent measured for ZnO-TAA-PbS is  $-89.1 \mu\text{A}/\text{cm}^2$ . As is the case for the preceding results, the ZnO-TAA-PbS shows different trends in comparison to all of the other molecular systems used in this study.

The photoresponse profile to a steady state on-off dc illumination (Figure 13) shows a very quick increase followed by a slight exponential decrease of the signal during light irradiation and also a quick return to zero upon switching off

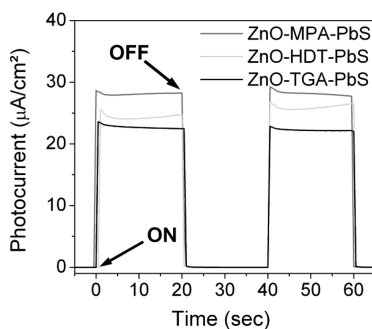


**Figure 13.** Typical photoresponse profile for three ZnO-linker-PbS systems.

the light. This optical response was found to be reproducible over many cycles (in the present study over many cycles) therefore providing an indication of the stability of the PbS derived ZnO substrates. Identification of the processes that exist in such systems and their kinetic pathways requires more complex analysis methods, and more complete analyses of several such sequences are presently in progress. These are expected to give clearer insights concerning many of the processes which occur and which cannot be clarified in the present study.

## CONCLUSIONS

In summary, therefore, monodisperse PbS and ZnO nanoparticles were synthesized and characterized using optical spectroscopy. The ZnO nanoparticles were deposited onto an ITO substrate by spin coating and subsequent annealing. Parameters were then determined which allowed the thickness of the ZnO layer on the ITO to be reproducible, and the ITO-ZnO substrates were characterized using SEM to confirm this reproducibility. The ITO-ZnO substrates were then treated with six different linking molecules (OA, MA, TAA, MPA, TGA, and HDT) onto which PbS could be attached. The resulting ITO-ZnO-linker systems were then probed using FTIR in order to determine the molecular linking modes and a mode of attachment to the ZnO proposed for each linker.

These substrates were further derivatized by immersion into a solution of PbS nanoparticles to provide an ITO-ZnO-linker-PbS system for further electrochemical and optoelectrochemical characterization using the techniques of CV, EIS, and photocurrent transients in order to gain insights into the role played by the linker molecules at the electrode interface in the mediation of charge transfer. First, cyclic voltammetry in sodium sulfite was employed to determine the potential range across which meaningful applied potential measurements could be performed. For ITO and ITO-ZnO substrates the background electrolyte underwent redox chemistry when a potential more negative than  $-1.2\text{ V}$  was applied using  $\text{Na}_2\text{SO}_3$  as electrolyte. For the ITO-ZnO-linker-PbS substrates, with the exception of those containing TAA, the cyclic voltammograms in  $\text{NaClO}_4$  displayed the rich electrochemistry associated with PbS, and a working potential window of approximately  $1.3\text{ V}$  from  $-0.8$  to  $+0.5$  in the dark was determined, which corresponds well with the NC band gap as determined optically. The electrochemical window for the NCs was wider than that associated with bulk galena which can be explained within the framework of quantum confinement.

To probe the changes in the solvent/substrate interfacial region in going from nonilluminated to illuminated conditions

EIS was employed. It was established that under conditions of illumination a shift in the phase to lower frequencies occurred, as did a decrease in the total resistance and an increase in the sum of the capacitances. A model was subsequently formulated to which the data could be fit with a high degree of accuracy. The photocurrent-response profile to a steady state on-off dc illumination shows a fast increase followed by a slight exponential decrease of the signal during light irradiation and also a quick return to zero upon switching off the light. This optical response was found to be reproducible over many cycles therefore providing an indication as to the stability of the PbS derived ZnO substrates.

## ASSOCIATED CONTENT

**S Supporting Information.** Table of the relevant FTIR band assignments, XRD, CV profiles, and the electrochemical impedance models and the values derived from them. This material is available free of charge via the Internet at <http://pubs.acs.org>.

## AUTHOR INFORMATION

### Corresponding Author

\*E-mail: s.hickey@chemie.tu-dresden.de. Website: <http://www.chm.tu-dresden.de/pc2/>.

## ACKNOWLEDGMENT

This work has been funded by the German Research Foundation (Deutsche Forschungsgemeinschaft (DFG)) through grant application HI-1113/3-1 and FP7 European union project INNOVASOL.

## REFERENCES

- (1) O'Regan, B.; Grätzel, M. *Nature* **1991**, *353*, 4.
- (2) Hara, K.; Horiguchi, T.; Kinoshita, T.; Sayama, K.; Sugihara, H.; Arakawa, H. *Sol. Energy Mater. Sol. Cells* **2000**, *64*, 115.
- (3) Nasr, C.; Hotchandani, S.; Kim, W. Y.; Schmehl, R. H.; Kamat, P. V. *J. Phys. Chem. B* **1997**, *101*, 7480.
- (4) Chappel, S.; Chen, S.-G.; Zaban, A. *Langmuir* **2002**, *18*, 3336.
- (5) Tennakone, K.; Kumara, G. R. R. A.; Kottekoda, I. R. M.; Perera, V. P. S. *Chem. Commun.* **1999**, 1.
- (6) Sayama, K.; Sugihara, H.; Arakawa, H. *Chem. Mater.* **1998**, *10*, 3825.
- (7) Chen, S. G.; Chappel, S.; Diamant, Y.; Zaban, A. *Chem. Mater.* **2001**, *13*, 4629.
- (8) Kroese, J. E.; Savenije, T. J. *Thin Solid Films* **2004**, *451–452*, 54.
- (9) Chen, Z.; Tang, Y.; Zhang, L.; Luo, L. *Electrochim. Acta* **2006**, *51*, 5870.
- (10) Xu, Y.; Schoonen, M. A. A. *Am. Mineral.* **2000**, *85*, 543.
- (11) Wei, S.-H.; Zunger, A. *Phys. Rev. B* **1997**, *55*, 13605.
- (12) Tudury, G. E.; Marquezini, M. V.; Ferreira, L. G.; Barbosa, L. C.; Cesar, C. L. *Phys. Rev. B* **2000**, *62*, 7357.
- (13) Wei, S.-H.; Zhang, S. B.; Zunger, A. *J. Appl. Phys.* **2000**, *87*, 1304.
- (14) Lade, S. J.; Upalane, M. D.; Lokhande, C. D. *Mater. Chem. Phys.* **2001**, *68*, 36.
- (15) Zhuravlev, K. K. *Phys. B* **2007**, *394*, 1.
- (16) Shen, Q.; Sato, T.; Hashimoto, M.; Chen, C.; Toyoda, T. *Thin Solid Films* **2006**, *499*, 299.
- (17) Kongkanand, A.; Tvrdy, K.; Takechi, K.; Kuno, M.; Kamat, P. V. *J. Am. Chem. Soc.* **2008**, *130*, 4007.

- (18) Lee, H. J.; Yum, J.-H.; Leventis, H. C.; Zakeeruddin, S. M.; Haque, S. A.; Chen, P.; Seok, S. I.; Grätzel, M.; Nazeeruddin, M. K. *J. Phys. Chem. C* **2008**, *112*, 11600.
- (19) Guijarro, N. s.; Lana-Villarreal, T.; Mora-Seró, I. n.; Bisquert, J.; Gómez, R. *J. Phys. Chem. C* **2009**, *113*, 4208.
- (20) Singh, R. S.; Rangari, V. K.; Sanagapalli, S.; Jayaraman, V.; Mahendra, S.; Singh, V. P. *Sol. Energy Mater. Sol. Cells* **2004**, *82*, 315.
- (21) Seabold, J. A.; Shankar, K.; Wilke, R. H. T.; Paulose, M.; Varghese, O. K.; Grimes, C. A.; Choi, K.-S. *Chem. Mater.* **2008**, *20*, 5266.
- (22) Lan, G.-Y.; Yang, Z.; Lin, Y.-W.; Lin, Z.-H.; Liao, H.-Y.; Chang, H.-T. *J. Mater. Chem.* **2009**, *19*, 6.
- (23) Lee, H. J.; Kim, D.-Y.; Yoo, J.-S.; Bang, J.; Kim, S.; Park, S.-M. *Bull. Korean Chem. Soc.* **2007**, *28*, 6.
- (24) Kamat, P. V. *J. Phys. Chem. C* **2007**, *111*, 2834.
- (25) Ellingson, R. J.; Beard, M. C.; Johnson, J. C.; Yu, P.; Micic, O. I.; Nozik, A. J.; Shabaev, A.; Efros, A. L. *Nano Lett.* **2005**, *5*, 865.
- (26) Shabaev, A.; Efros, A. L.; Nozik, A. J. *Nano Lett.* **2006**, *6*, 2856.
- (27) Klimov, V. I. *Annu. Rev. Phys. Chem.* **2007**, *58*, 635.
- (28) Schaller, R. D.; Sykora, M.; Pietryga, J. M.; Klimov, V. I. *Nano Lett.* **2006**, *6*, 424.
- (29) Werner, J. H.; Kolodinski, S.; Queisser, H. *J. Phys. Rev. Lett.* **1994**, *72*, 3851.
- (30) De Vos, A.; Desoete, B. *Sol. Energy Mater. Sol. Cells* **1998**, *51*, 413.
- (31) Oron, D.; Kazes, M.; Shweky, I.; Banin, U. *Phys. Rev. B* **2006**, *74*, 115333.
- (32) Vogel, R.; Hoyer, P.; Weller, H. *J. Phys. Chem.* **1994**, *98*, 3183.
- (33) Kamat, P. V. *J. Phys. Chem. C* **2008**, *112*, 18737.
- (34) Guijarro, N. s.; Shen, Q.; Giménez, S.; Mora-Seró, I. n.; Bisquert, J.; Lana-Villarreal, T.; Toyoda, T.; Gómez, R. *J. Phys. Chem. C* **2010**, *114*, 22352.
- (35) Watson, D. F. *J. Phys. Chem. Lett.* **2010**, *1*, 2299.
- (36) Spanhel, L.; Anderson, M. A. *J. Am. Chem. Soc.* **1991**, *113*, 2826.
- (37) Meulenkamp, E. A. *J. Phys. Chem. B* **1998**, *102*, 5566.
- (38) Hickey, S. G.; Riley, D. J. *J. Phys. Chem. B* **1999**, *103*, 4599.
- (39) Hickey, S. G.; Riley, D. J. *Electrochim. Acta* **2000**, *45*, 3277.
- (40) Doherty, R. P.; Hickey, S. G.; Riley, D. J.; Tull, E. J. *J. Electroanal. Chem.* **2004**, *569*, 271.
- (41) Fermín, D. J.; Ponomarev, E. A.; Peter, L. M. *J. Electroanal. Chem.* **1999**, *473*, 192.
- (42) Peter, L. M.; Riley, D. J.; Tull, E. J.; Wijayantha, K. G. U. *Chem. Commun.* **2002**, 1030.
- (43) Sagar, P.; Shishodia, P. K.; Mehra, R. M.; Okada, H.; Wakahara, A.; Yoshida, A. *J. Lumin.* **2007**, *126*, 800.
- (44) Özgür, U.; Alivov, Y. I.; Liu, C.; Teke, A.; Reshchikov, M. A.; Dogan, S.; Avrutin, V.; Cho, S.-J.; Morkoc, H. *J. Appl. Phys.* **2005**, *98*, 041301.
- (45) Noack, V.; Eychmüller, A. *Chem. Mater.* **2002**, *14*, 1411.
- (46) Noack, V.; Weller, H.; Eychmüller, A. *J. Phys. Chem. B* **2002**, *106*, 8514.
- (47) Imae, T.; Torii, H. *J. Phys. Chem. B* **2000**, *104*, 9218.
- (48) Redington, R. L.; Redington, T. E. *J. Mol. Struct.* **1978**, *48*, 165.
- (49) Hug, S. J.; Sulzberger, B. *Langmuir* **1994**, *10*, 3587.
- (50) Degenhardt, J.; McQuillan, A. J. *Chem. Phys. Lett.* **1999**, *311*, 179.
- (51) Specht, C. H.; Frimmel, F. H. *J. Mol. Struct.* **2001**, *3*, 6.
- (52) Shippey, T. A. *J. Mol. Struct.* **1980**, *65*, 71.
- (53) Hanrahan, E. S. *Spectrochim. Acta* **1966**, *22*, 1243.
- (54) Sheppard, N. *Trans. Faraday Soc.* **1949**, *45*, 5.
- (55) Cefola, M.; Peter, S. S.; Gentile, P. S.; Celiano, R. A. V. *Talanta* **1962**, *9*, 537.
- (56) Bumm, L. A.; Arnold, J. J.; Dunbar, T. D.; Allara, D. L.; Weiss, P. S. *J. Phys. Chem. B* **1999**, *103*, 8122.
- (57) Dibbell, R. S.; Watson, D. F. *J. Phys. Chem. C* **2009**, *113*, 3139.
- (58) Holmlin, R. E.; Ismagilov, R. F.; Haag, R.; Mujica, V.; Ratner, M. A.; Rampi, M. A.; Whitesides, G. M. *Angew. Chem., Int. Ed.* **2001**, *40*, 5.
- (59) Sumner, J. J.; Weber, K. S.; Hockett, L. A.; Creager, S. E. *J. Phys. Chem. B* **2000**, *104*, 7449.
- (60) Ganesh, V.; Lakshminarayanan, V. *Langmuir* **2006**, *22*, 1561.
- (61) Slowinski, K.; Chamberlain, R. V.; Miller, C. J.; Majda, M. *J. Am. Chem. Soc.* **1997**, *119*, 11910.
- (62) Rifai, S.; Lopinski, G. P.; Ward, T.; Wayner, D. D. M.; Morin, M. *Langmuir* **2003**, *19*, 8916.
- (63) Paul, R. L.; Nicol, M. J.; Diggle, J. W.; Saunders, A. P. *Electrochim. Acta* **1978**, *23*, 625.
- (64) Davis, A. P.; Huang, C. P. *Langmuir* **1991**, *7*, 803.
- (65) Gardner, J. R.; Woods, R. J. *Electroanal. Chem.* **1979**, *100*, 447.
- (66) Mikhlin, Y. J. *Appl. Electrochem.* **2004**, *34*, 37.
- (67) Nicol, M. J.; Paul, R. L.; Diggle, J. W. *Electrochim. Acta* **1978**, *23*, 635.
- (68) Ogawa, S.; Hu, K.; Fan, F.-R. F.; Bard, A. J. *J. Phys. Chem. B* **1997**, *101*, 5707.
- (69) Chernyshova, I. V. *Russ. J. Electrochim.* **2001**, *37*, 579.
- (70) Pauporté, T.; Schuhmann, D. J. *Electroanal. Chem.* **1996**, *404*, 123.
- (71) Haram, S. K.; Quinn, B. M.; Bard, A. J. *J. Am. Chem. Soc.* **2001**, *123*, 8860.
- (72) Poznyak, S. K.; Osipovich, N. P.; Shavel, A.; Talapin, D. V.; Gao, M.; Eychmüller, A.; Gaponik, N. *J. Phys. Chem. B* **2005**, *109*, 1094.
- (73) Brus, L. E. *J. Chem. Phys.* **1984**, *80*, 4403.
- (74) Bard, A. J.; Faulkner, L. R. *Electrochemical Methods: Fundamentals and Applications*, 2nd ed.; John Wiley & Sons: New York, 2001.
- (75) Moser, J.; Punchihewa, S.; Infelta, P. P.; Graetzel, M. *Langmuir* **1991**, *7*, 3012.
- (76) Rühle, S.; Greenshtein, M.; Chen, S. G.; Merson, A.; Pizem, H.; Sukenik, C. S.; Cahen, D.; Zaban, A. *J. Phys. Chem. B* **2005**, *109*, 18907.